

Sulphate adsorption at the Fe (hydr)oxide–H₂O interface: comparison of cluster and periodic slab DFT predictions

K. W. PAUL^a, J. D. KUBICKI^b & D. L. SPARKS^a

^aDepartment of Plant and Soil Sciences, University of Delaware, Newark, Delaware 19717, and ^bDepartment of Geosciences and Earth and Environmental Systems Institute, The Pennsylvania State University, University Park, Pennsylvania 16802, USA

Summary

The transport and bioavailability of sulphate in soils are significantly affected by adsorption reactions at the mineral–H₂O interface. Therefore, an understanding of the mechanisms and kinetics of sulphate adsorption is of fundamental importance in soil chemistry. In this investigation, the binding geometries of bidentate bridging and monodentate sulphate complexes at the Fe (hydr)oxide–H₂O interface were predicted with static cluster and periodic slab density functional theory (DFT) calculations. The cluster calculations were performed with edge-sharing dioctahedral Fe³⁺ models, using the unrestricted PBE0 exchange–correlation functional and a combination of effective core potential (LanL2DZ – Fe atoms) and all-electron (6–311+G(d,p) or 6–311+G(3df,p) – S, O, and H atoms) basis sets. The periodic slab calculations were performed with a (3 × 2) slab of the (100) α -FeOOH surface, by means of the projector-augmented wave method and a plane-wave basis set. For the periodic slab DFT calculations, the spin-polarized (SP) PBE exchange–correlation functional, with and without explicit consideration of an on-site Coulomb interaction parameter (i.e. SP-PBE and SP-PBE+U methods), was used. Despite the lack of long-range order, cluster model predictions of the interatomic distances and angles of bidentate bridging and monodentate sulphate were in good agreement with the periodic slab model predictions. Quantitative analysis of the cluster and periodic slab DFT predictions is expected to result from theoretical fitting of extended X-ray absorption fine structure measurements. The application of computational chemistry methods to soil chemistry research is anticipated to provide novel insight into the mechanisms and kinetics of ion sorption.

Introduction

The transport and bioavailability of sulphate in soils are significantly affected by adsorption reactions with metal oxides and clay minerals. In tropical soils that possess appreciable anion exchange capacity (AEC), for example, variably-charged Al and Fe (hydr)oxides and 1:1 clay minerals (e.g. kaolinite) can retain plant-available sulphate through adsorption. In soils that do not possess appreciable AEC, however, sulphate can become unavailable for plant uptake due to leaching through the soil profile (Sparks, 2003). Therefore, an understanding of the mechanisms and kinetics of sulphate adsorption is of fundamental importance in soil chemistry. In particular, determining the mechanisms of sulphate adsorption will help to constrain surface complexation models, which can be used to simulate the reactive transport of chemical species in soils.

Spectroscopic measurements can provide valuable molecular-scale information with respect to the mechanisms and kinetics of sulphate adsorption. Unfortunately, the initial adsorption reactions of sulphate, and other oxyanions such as phosphate and arsenate, can reach steady-state rapidly (e.g. < 1 ms) (Sparks, 2003). As a result, it is challenging to perform high-resolution spectroscopic measurements necessary to identify reaction intermediates and to determine the kinetics of a reaction (Brown & Sturchio, 2002). In addition, spectroscopic studies often use inconsistent experimental designs and data analysis protocols, which can lead to conflicting interpretations. Consequently, it remains difficult to systematically test and validate proposed reaction mechanisms based upon spectroscopic measurements. In this respect, computational chemistry methods can provide novel insight into the mechanisms and kinetics of adsorption reactions. For example, computational chemistry methods can be used to interpret spectroscopic measurements, predict adsorption rate constants and activation barriers, and to estimate the energies of adsorption reactions.

Correspondence: K. W. Paul. E-mail: kpaul@udel.edu
Received 3 February 2006; revised version accepted 21 May 2007

Computational chemistry methods have been used recently to investigate the adsorption of oxyanions and organic acids on Al and Fe (hydr)oxides, particularly to interpret extended X-ray absorption fine structure (EXAFS) and Fourier transform infrared (FTIR) spectroscopic measurements (Ladeira *et al.*, 2001; Sherman & Randall, 2003; Kwon & Kubicki, 2004; Omoike *et al.*, 2004; Yoon *et al.*, 2004; Bargar *et al.*, 2005; Paul *et al.*, 2005; Persson & Axe, 2005; Zhang *et al.*, 2005; Baltrusaitis *et al.*, 2006; Tribe *et al.*, 2006;). In general, density functional theory (DFT) calculations were performed with edge-sharing dioctahedral Al^{3+} or Fe^{3+} cluster models (exceptions included Yoon *et al.*, 2004; Persson & Axe, 2005; Baltrusaitis *et al.*, 2006). For example, Sherman & Randall (2003) investigated the adsorption of arsenate (As(V)) on Fe (hydr)oxides, using a combination of EXAFS spectroscopy and DFT cluster model calculations. Previous EXAFS studies had proposed conflicting binding geometries for As(V) complexes on Fe (hydr)oxides, including bidentate bridging, bidentate chelating, and monodentate (Sherman & Randall, 2003, and references therein). The DFT cluster model calculations predicted that the most thermodynamically favourable adsorption product was a bidentate bridging As(V) complex. EXAFS measurements of the As(V)–Fe interatomic distance agreed well with the bidentate bridging As(V) cluster model, which corroborated the thermodynamic DFT prediction (Sherman & Randall, 2003).

As another example, Paul *et al.* (2005) investigated the effect of hydration on sulphate adsorption and speciation at the Fe (hydr)oxide– H_2O interface, with a combination of attenuated total reflectance (ATR) FTIR spectroscopy and DFT cluster model calculations. DFT calculations of IR vibrational frequencies predicted that sulphate formed a bidentate bridging or monodentate complex at the Fe (hydr)oxide– H_2O interface. Under dehydrated conditions, however, the DFT calculations predicted that a speciation change would occur. Specifically, sulphate probably accepts a proton to form a bidentate bridging or monodentate bisulphate complex. The results reported by the investigation of Paul *et al.* (2005) were important because the moisture content of soils is in constant fluctuation. Fluctuations of soil moisture content may affect nutrient transport and bioavailability, but unfortunately our understanding of this natural process remains limited.

DFT cluster model calculations of oxyanion and organic acid complexes have been valuable for predicting and interpreting EXAFS and FTIR spectroscopic measurements. However, previous DFT studies have generally relied on edge-sharing dioctahedral Al^{3+} and Fe^{3+} cluster models to simulate the surfaces of Al and Fe (hydr)oxide minerals. It is reasonable to assume that edge-sharing dioctahedral cluster models cannot accurately predict the binding geometries of oxyanion and organic acid complexes on every surface of a soil mineral. Common soil minerals, for example goethite (α -FeOOH), possess several surfaces with unique structures and compositions (e.g. the (101) and (001) α -FeOOH surfaces; Gaboriaud & Ehrhardt, 2003). Consequently, complications may arise if the geometry-

optimized structures of edge-sharing dioctahedral cluster models inaccurately predict binding geometries (e.g. interatomic distances). An alternative approach is to model a soil mineral surface as a periodic slab (i.e. a two-dimensional periodic surface constrained by boundary conditions). Unfortunately, few studies have used periodic slab models to investigate the adsorption of nutrients at the mineral– H_2O interface.

The objective of this investigation was to compare the binding geometries of inner-sphere sulphate complexes predicted by cluster and by periodic slab DFT calculations. The DFT cluster calculations were performed with edge-sharing dioctahedral Fe^{3+} models. The periodic slab DFT calculations were performed with a (3×2) slab of the (100) α -FeOOH surface. Goethite is the most abundant iron oxyhydroxide in soils. Furthermore, the (100) α -FeOOH surface possesses a similar structure and composition to the edge-sharing dioctahedral Fe^{3+} cluster models. The periodic slab DFT calculations account realistically for long-range order and should therefore predict accurate binding geometries. This investigation is also part of an ongoing research effort to analyse how well DFT models of sulphate complexes fit experimental EXAFS measurements. This investigation will demonstrate that DFT cluster models of inner-sphere sulphate complexes compare reasonably well with similar periodic slab DFT models, despite their lack of long-range order.

Computational methods

Cluster model calculations

The local binding geometries of inner-sphere sulphate complexes were predicted, using static configurations of edge-sharing dioctahedral Fe^{3+} cluster models. Edge-sharing dioctahedral cluster models of metal cations (e.g. Al^{3+} and Mg^{2+}) have been shown to reproduce accurately the main geometrical features of metal oxides and clay minerals (Sainz-Diaz *et al.*, 2000). Similar cluster models have also been used to analyse the local binding geometries of inner-sphere As(V) complexes on gibbsite (Ladeira *et al.*, 2001) and Fe (hydr)oxide minerals (Sherman & Randall, 2003), as well as inner-sphere arsenite (As(III)) complexes on goethite (Manning *et al.*, 1998; Zhang *et al.*, 2005), based upon EXAFS measurements. In this investigation, bidentate bridging and monodentate sulphate complexes were modelled. Bidentate bridging and monodentate sulphate are the most common inner-sphere complexes proposed by spectroscopic studies (Parfitt & Smart, 1977, 1978; Harrison & Berkheiser, 1982; Turner & Kramer, 1991; Watanabe *et al.*, 1994; Hug, 1997; Peak *et al.*, 1999; Wijnja & Schulthess, 2000; Paul *et al.*, 2005).

The overall charge of each edge-sharing dioctahedral Fe^{3+} -sulphate cluster model was neutral (i.e. +2 charged edge-sharing dioctahedral Fe^{3+} cluster and –2 charged sulphate). Therefore, the cluster model calculations simulated adsorption below the pH_{pzc} (pH_{pzc} is defined as the pH at which the net

surface charge density equals zero; Sposito, 1998). To simulate a hydrated environment, several explicit H₂O molecules (i.e. H₂O molecules included in the geometry optimization) were H-bonded to the sulphate complexes. Experimental studies have shown that hydration significantly influences the IR-active vibrational modes of oxyanion complexes (Hug, 1997; Myneni *et al.*, 1998). For bidentate bridging sulphate, cluster model calculations were performed with four or 10 explicit H₂O molecules (Figures 1 and 4). For monodentate sulphate, cluster model calculations were performed with six or 10 explicit H₂O molecules (Figures 1 and 4). In addition, the bidentate bridging sulphate cluster model containing four explicit H₂O molecules was geometry-optimized with the Integral Equation Formalism Polarized Continuum Model (IEFPCM) method (Cances *et al.*, 1997). For the IEFPCM calculation, the dielectric constant of bulk water ($\epsilon = 78.4$) was specified, and therefore both explicit and implicit solvation were considered.

The DFT cluster model calculations were performed with Gaussian 03 (Frisch *et al.*, 2003). The DFT calculations were performed with the unrestricted, hybrid exchange-correlation functional of Perdew *et al.* (1996), denoted UPBE0. The LanL2DZ effective core potential (ECP) basis set (Hay & Wadt, 1985) was used for the Fe atoms. The high-spin state of Fe³⁺ was specified for each Fe atom. The 6-311+G(d,p) or 6-311+G(3df,p) all-electron basis sets were used for the S, O, and H atoms. It should be noted that several other exchange-correlation functionals and basis sets were evaluated. For the purposes of this investigation, however, only the UPBE0 predictions are reported because of their comparatively closer agreement with the periodic slab DFT predictions. Numerous DFT investigations have used similar clusters to model oxyanion and organic acid complexes on Al or Fe (hydr)oxides, and successfully compared the predictions to experimental measurements (Ladeira *et al.*, 2001; Sherman & Randall, 2003; Kwon & Kubicki, 2004; Omoike *et al.*, 2004; Yoon *et al.*, 2004; Bargar *et al.*, 2005; Paul *et al.*, 2005, 2006; Persson & Axe, 2005; Zhang *et al.*, 2005; Baltrusaitis *et al.*, 2006; Tribe *et al.*, 2006).

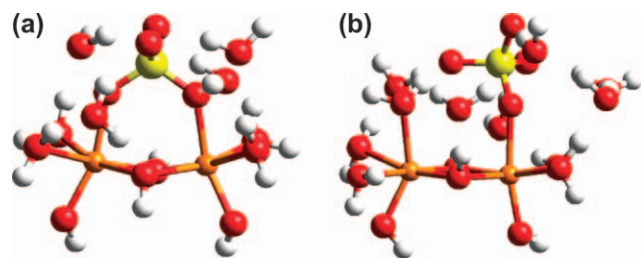


Figure 1 Geometry-optimized inner-sphere sulphate complexes on edge-sharing dioctahedral Fe³⁺ cluster models: (a) bidentate bridging sulphate (Fe₂(OH)₄(OH₂)₄SO₄·(H₂O)₄) and (b) monodentate sulphate (Fe₂(OH)₄(OH₂)₅SO₄·(H₂O)₆). Explicit H₂O molecules are H-bonded to the sulphate complexes. Red, oxygen; white, hydrogen; yellow, sulphur; orange, iron.

The starting configurations for the bidentate bridging (four explicit H₂O molecules) and monodentate (six explicit H₂O molecules) sulphate complexes corresponded to energy-minimized cluster models from a previous investigation (Paul *et al.*, 2006). The cluster models were geometry-optimized without symmetry or geometrical constraints. Frequency calculations were subsequently performed to determine whether the geometry optimization had successfully located a potential energy minimum (i.e. no imaginary frequencies). It should be noted, however, that only one configuration was geometry-optimized for each cluster model. Therefore, the potential energy minima were unlikely to correspond to the global minima for these configurations (i.e. conformational analysis of the potential energy surfaces was not performed).

Periodic slab model calculations

The unit cell of bulk α -FeOOH (*Pnma* space group) was constructed in Cerius² (Accelrys Inc., San Diego, California) according to the experimental lattice parameters and atomic coordinates published by Szytula *et al.* (1968). The unit cell of bulk α -FeOOH was cleaved through the (100) plane ((010) plane in the *Pbnm* space group; Hahn, 1996), corresponding to a depth of one unit cell. The (100) surface is a stable low-index surface of α -FeOOH (Cornell *et al.*, 1974). A slab model of the (100) α -FeOOH surface was constructed, corresponding to a quasi-cubic slab with lattice vectors $a = 9.03$, $b = 9.24$, and $c = 8.89$ Å (i.e. a (3×2) slab). The (100) α -FeOOH surface was exposed equivalently on both sides of the slab. Periodic images of the slab perpendicular to the (100) α -FeOOH surface (i.e. a - b plane) were separated by a vacuum space of approximately 10 Å ($c = 18.89$ Å).

Cleavage of bulk α -FeOOH through the (100) plane resulted in surface Fe atoms with 5-fold coordination. These surface Fe atoms were terminated with singly-coordinated OH₂ functional groups. The overall charge of the (100) α -FeOOH slab was stoichiometrically neutral (Fe₂₄O₆₀H₄₈). The vacuum space was subsequently filled with explicit H₂O molecules (including the one or two singly-coordinated OH₂ functional groups replaced by the SO₄²⁻ ligand), corresponding to a density of approximately 0.95 g cm⁻³. One Ca²⁺ cation was also added to maintain a neutrally-charged simulation cell and to simulate the presence of a counterion. Starting configurations for the inner-sphere sulphate complexes on the (100) α -FeOOH surface (e.g. bond distances and angles) were approximately equal to the energy-minimized configurations predicted by the DFT cluster model calculations.

The periodic slab DFT calculations were performed with the Vienna *ab initio* simulation package (VASP) (Kresse & Furthmüller, 1996a, b). VASP is a DFT electronic structure program that solves the Kohn-Sham equations (Kohn & Sham, 1965), using pseudopotentials or the projector-augmented wave method and a plane-wave basis set. The exchange-correlation functional chosen was the spin-polarized generalized

gradient approximation (SP-GGA) functional of Perdew *et al.* (1996), denoted SP-PBE. The Kohn-Sham equations were solved by minimizing the norm of the residual vector to each eigenstate and efficient charge- and spin-mixing routines (Pulay, 1980; Wood & Zunger, 1985).

The electron-ion interactions were described by the projector-augmented wave method of Blöchl (1994), as implemented by Kresse & Joubert (1999). The number of valency electrons treated explicitly for each heavy element was as follows: Fe, $3p^6 3d^7 4s^1$; O, $2s^2 2p^4$; S, $3s^2 3p^4$. Brillouin zone sampling was performed automatically through implementation of the Monkhorst-Pack scheme (Monkhorst & Pack, 1976). The reciprocal space of the Brillouin zone was subdivided into a $2 \times 2 \times 1$ mesh, which resulted in two k -points that sampled the irreducible part of the Brillouin zone. The plane-wave kinetic energy cutoff was set to 400 eV. The atomic positions were relaxed using a conjugate-gradient algorithm. The geometry optimizations were considered completed when the Hellmann-Feynman forces acting on the atoms were less than $0.02 \text{ eV } \text{Å}^{-1}$ and the error in total energy was less than 10^{-4} eV . All of the atomic positions were allowed to relax, but the shape and size of the simulation cell were conserved. The geometry optimizations were performed with a first-order Gaussian smearing coefficient, σ , of 0.10 eV (Methfessel & Paxton, 1989).

At room temperature, α -FeOOH is known to be an antiferromagnetic mineral. In this investigation, the number of unpaired valency electrons initially specified for each Fe atom corresponded to five (i.e. high-spin state of Fe^{3+}). Unfortunately, SP-GGA methods can fail to describe correctly the strong electronic correlations of valency electrons in transition metal atoms. Therefore, the periodic slab DFT calculations were performed with both the SP-GGA and SP-GGA+U methods. In both cases, the GGA functional corresponded to the SP-PBE exchange-correlation functional.

The SP-GGA+U method considers explicitly the on-site Coulomb repulsion for strongly correlated d- and f-electrons. In the SP-GGA+U method, a Hubbard term describing the on-site Coulomb and exchange interactions is added to the DFT Hamiltonian. Explicit consideration of the on-site Coulomb repulsion has been shown to improve significantly predictions of the local magnetic moments of Fe atoms, band gaps, and band energies for bulk haematite (α - Fe_2O_3) (Rollmann *et al.*, 2004). For a description of the SP-GGA+U method applied to the closely related α - Fe_2O_3 system, refer to Rollmann *et al.* (2004). Dudarev's rotationally-invariant approach to the SP-GGA+U method was used in this investigation (Dudarev *et al.*, 1998). The effective on-site Coulomb and exchange interaction parameters for each Fe atom were set to 4 eV and 1 eV, respectively, as recommended by Rollmann *et al.* (2004).

Results and discussion

The adsorption of sulphate at the Al and Fe (hydr)oxide- H_2O interface has received significant attention in the literature. In

particular, several studies have published results from *in situ* ATR-FTIR spectroscopic measurements (Hug, 1997; Eggleston *et al.*, 1998; Peak *et al.*, 1999; Wijnja & Schulthess, 2000; Paul *et al.*, 2005). For example, Hug (1997) performed ATR-FTIR spectroscopic measurements of sulphate adsorbed at the α - Fe_2O_3 - H_2O interface as a function of pH and hydration. Interestingly, a diagnostic IR-active vibrational mode $\geq 1200 \text{ cm}^{-1}$ was only observed when the ATR-FTIR measurements were performed on dehydrated samples (i.e. *ex situ*). The diagnostic IR-active vibrational mode was also observed with sulphate solutions acidified below pH 2 (i.e. less than the pK_a of HSO_4^-). Hug (1997) proposed that sample dehydration may alter the coordination or speciation of an inner-sphere sulphate complex. Paul *et al.* (2005) subsequently showed with DFT cluster model calculations that sample dehydration probably results in bisulphate formation (i.e. a change in sulphate speciation).

The application of *in situ* ATR-FTIR spectroscopy to the investigation of oxyanion adsorption at the mineral- H_2O interface is not without its limitations. One principal limitation is that a point group symmetry analysis of the IR-active vibrational modes is generally performed to determine the binding geometry of an oxyanion complex (e.g. monodentate or bidentate). Hence, IR spectroscopy has been referred to as an 'indirect structural' method (Waychunas *et al.*, 2005). Unfortunately, the IR-active vibrational modes of an oxyanion complex are usually broad and overlapping. Consequently, identifying the exact number of IR-active vibrational modes remains challenging and interpretations can be inconclusive. For example, Paul *et al.* (2005) found that the DFT-predicted ν_1 and ν_3 IR-active vibrational frequencies of monodentate and bidentate bridging sulphate had relatively similar energies. Assuming that the correct number of experimentally measured IR-active vibrational modes was identified, it was reasonable to propose either a monodentate or bidentate bridging sulphate complex (Hug, 1997; Paul *et al.*, 2005). Furthermore, although bisulphate probably formed on α - Fe_2O_3 as a function of dehydration, differentiating between the monodentate and bidentate bridging bisulphate complexes proved impossible (predicted IR-active vibrational frequencies were indistinguishable).

EXAFS is an alternative *in situ* spectroscopic method often used to investigate oxyanion adsorption at the mineral- H_2O interface. However, in contrast to IR spectroscopy, EXAFS is a 'direct structural' method (Waychunas *et al.*, 2005). An EXAFS analysis typically provides the interatomic distances between a central absorbing atom and its next-nearest neighbours (e.g. first and second shells). Furthermore, the coordination numbers of the first and second shells can be estimated. In principle, EXAFS spectroscopy is capable of differentiating between monodentate and bidentate bridging complexes, assuming their second shell interatomic distances and coordination numbers are sufficiently different (e.g. Fendorf *et al.*, 1997). To determine the binding geometry of an oxyanion

complex at the mineral–H₂O interface, EXAFS analyses typically employ standard reference compounds as structural models for EXAFS fitting. A promising alternative is to derive structural models from DFT cluster calculations (e.g. Persson & Axe, 2005). DFT-predicted structural models of oxyanion complexes can be used to calculate photoelectron scattering amplitudes and phase shifts necessary for EXAFS fitting.

Recently, we initiated an investigation into the adsorption of sulphate at the Fe (hydr)oxide–H₂O interface, using a combination of S *K*-edge EXAFS spectroscopy and DFT model calculations. A primary goal of this research effort is to fit the EXAFS measurements with DFT-predicted structural models of sulphate complexes. In this respect, it is particularly worthwhile to quantify the potential differences between cluster and periodic slab DFT predictions. Several researchers have used DFT-predicted cluster models of adsorption complexes to interpret bulk EXAFS measurements (Ladeira *et al.*, 2001; Sherman & Randall, 2003; Persson & Axe, 2005; Zhang *et al.*, 2005). In addition, a growing number of metal and oxyanion adsorption studies are being performed with single-crystal mineral surfaces, using grazing incidence (GI) EXAFS and crystal truncation rod (CTR) diffraction measurements (e.g. Bargar *et al.*, 2004; Catalano *et al.*, 2005; Waychunas *et al.*, 2005). For these studies DFT-predicted periodic slab models are anticipated to be valuable.

Tables 1 and 2 list selected interatomic distances and angles corresponding to the bidentate bridging and monodentate sulphate complexes, predicted by the cluster and periodic slab DFT calculations, respectively. The geometry-optimized cluster and periodic slab DFT models are displayed in Figures 1–3. It should be noted that the periodic slab SP-PBE and SP-PBE+U calculations did not result in significant differences regarding the predicted interatomic distances and angles of the sulphate

complexes (Table 2). As expected, however, differences were predicted for the average local magnetic moments of the individual Fe atoms. The average local magnetic moment was 3.65 μ_B Fe⁻¹ atom ($\pm 0.03 \mu_B$) and 4.09 μ_B Fe⁻¹ atom ($\pm 0.01 \mu_B$) for the SP-PBE and SP-PBE+U geometry-optimized configurations, respectively. Nevertheless, differences in the average local magnetic moments of the individual Fe atoms did not significantly affect the binding geometries of the sulphate complexes.

The binding geometry of the bidentate bridging sulphate complex will be discussed first. Overall, the cluster and periodic slab DFT predictions of the interatomic distances and angles were in good agreement, with only a few notable exceptions (Tables 1 and 2). In EXAFS analysis, a diagnostic feature of the binding geometry of an oxyanion complex is its second shell interatomic distance (e.g. the S–Fe interatomic distance). The average S–Fe interatomic distance predicted by the cluster (3.25 Å, LanL2DZ/6–311+G(3df,p)) and periodic slab (3.29 Å) DFT calculations agreed to within 0.04 Å, approximately equal to experimental error (Brown & Sturchio, 2002) (Tables 1 and 2). The predicted average S–O and S–O(Fe) bond distances (i.e. the first shell bond distances of S) were also in good agreement. The average S–O bond distance predicted by the cluster and periodic slab DFT calculations was 1.46 and 1.49 Å, respectively. Likewise, the average S–O(Fe) bond distance predicted by both the cluster and periodic slab DFT calculations was 1.49 Å (Tables 1 and 2).

One notable discrepancy between the cluster and periodic slab DFT predictions was the average (S)O–Fe bond distance of bidentate bridging sulphate. The average (S)O–Fe bond distance predicted by the edge-sharing dioctahedral Fe³⁺ cluster model was 2.03 Å (Table 1). On the other hand, the average (S)O–Fe bond distance predicted by the periodic (100) α -FeOOH slab

Table 1 Geometry-optimized bidentate bridging and monodentate sulphate complexes on an edge-sharing dioctahedral Fe³⁺ cluster model. Interatomic distances are reported in angstroms (Å) and bond angles in degrees. *Denotes interatomic distances and angles within the Fe–O–Fe–O ring between the two edge-sharing Fe³⁺ octahedra coordinated to sulphate

	Bidentate SO ₄ ²⁻ Fe ₂ (OH) ₄ (OH) ₂ SO ₄ ·(H ₂ O) ₄		Monodentate SO ₄ ²⁻ Fe ₂ (OH) ₄ (OH) ₂ SO ₄ ·(H ₂ O) ₆	
	LanL2DZ/ 6–311+G(d,p)	LanL2DZ/ 6–311+G(3df,p)	LanL2DZ/ 6–311+G(d,p)	LanL2DZ/ 6–311+G(3df,p)
Distance/Å				
S–Fe	3.27	3.25	3.46	3.49
S–O	1.48	1.46	1.50 (± 0.02)	1.48 (± 0.02)
S–O(Fe)	1.51	1.49	1.51	1.49
(S)O–Fe	2.03	2.03	2.12	2.14
Fe–Fe ^{*a}	3.08	3.02	3.00	2.95
Fe–O ^{*b}	2.03 (± 0.04)	2.01 (± 0.03)	1.98 (± 0.05)	1.96 (± 0.05)
Angle/degrees				
S–O–Fe	134.5	134.1	144.7	147.3
O–Fe–O*	78.8	80.3	81.2	82.6
Fe–O–Fe*	98.9	97.4	98.8	97.4

^aExperimental bulk Fe–Fe interatomic distances in Fe (hydr)oxides along single, edge-sharing dioctahedral chains range from approximately 2.96 to 3.07 Å.

^bExperimental bulk Fe–O and Fe–O(H) bonds bridging two Fe³⁺ octahedra range from approximately 1.89 to 2.12 Å (Waychunas *et al.*, 1996).

Table 2 Geometry-optimized bidentate bridging and monodentate sulphate complexes on a hydrated (100) α -FeOOH surface slab. Interatomic distances are reported in angstroms (\AA) and bond angles in degrees. *Denotes local interatomic distances and angles within the Fe–O–Fe–O ring between two edge-sharing Fe^{3+} octahedra coordinated to sulphate (monodentate values are averaged from two pairs of adjacent edge-sharing Fe^{3+} octahedra)

	Bidentate SO_4^{2-}		Monodentate SO_4^{2-}	
	SP-PBE	SP-PBE+U	SP-PBE	SP-PBE+U
Distance/ \AA				
S–Fe	3.29	3.29	3.48	3.47
S–O	1.49	1.49	1.50 (\pm 0.01)	1.50 (\pm 0.01)
S–O(Fe)	1.49	1.49	1.48	1.48
(S)O–Fe	2.16	2.15	2.18	2.16
Fe–Fe* ^a	2.99	2.99	3.02	3.02
Fe–O* ^b	2.03 (\pm 0.05)	2.03 (\pm 0.04)	2.04 (\pm 0.06)	2.04 (\pm 0.05)
Angle/degrees				
S–O–Fe	127.5	128.0	142.9	143.5
O–Fe–O*	84.7	85.0	83.7 (\pm 0.3)	84.1 (\pm 0.4)
Fe–O–Fe*	95.2	95.1	95.9 (\pm 3.6)	95.7 (\pm 3.1)

^aExperimental bulk Fe–Fe interatomic distances in Fe (hydr)oxides along single, edge-sharing dioctahedral chains range from approximately 2.96 to 3.07 \AA .

^bExperimental bulk Fe–O and Fe–O(H) bonds bridging two Fe^{3+} octahedra range from approximately 1.89 to 2.12 \AA (Waychunas *et al.*, 1996).

model was 2.15–2.16 \AA (Table 2). This significant disagreement was probably related to differences in the treatment of hydration. For the geometry optimization of bidentate bridging sulphate on the edge-sharing dioctahedral Fe^{3+} cluster model (Figure 1), only four explicit H_2O molecules were included. Conversely, 20 explicit H_2O molecules were included in the (100) α -FeOOH slab model, corresponding to a density of approximately 0.95 g cm^{-3} (Figure 2). In the latter model, the sulphate complex was completely hydrated. The effects of explicit and implicit solvation on the DFT-predicted (S)O–Fe bond distances of bidentate bridging sulphate will be discussed shortly.

Tables 1 and 2 also list the predicted interatomic distances and angles within the Fe–O–Fe–O ring between two edge-sharing Fe^{3+} octahedra, which are qualitatively comparable to bulk EXAFS and X-ray diffraction measurements. Measurements of Fe–Fe interatomic distances in Fe (hydr)oxide minerals are generally associated with dioctahedral Fe^{3+} chains (and single octahedral Fe^{3+} chains) along, across, and between the neighbouring chains (Waychunas *et al.*, 1996). The Fe–Fe interatomic distance measured along a dioctahedral Fe^{3+} chain ranges from approximately 2.96 to 3.07 \AA , while the Fe–Fe interatomic distance measured across a dioctahedral Fe^{3+} chain ranges from approximately 3.29 to 3.31 \AA (Waychunas *et al.*, 1996). The Fe–Fe interatomic distance measured between neighbouring dioctahedral Fe^{3+} chains ranges from approximately 3.36 to 4.00 \AA (e.g. corner-sharing Fe^{3+} octahedra). The Fe–O and Fe–O(H) bonds bridging two Fe^{3+} octahedra range from approximately 1.89 to 2.12 \AA (exceptions include β -FeOOH and ferrihydrite) (Waychunas *et al.*, 1996).

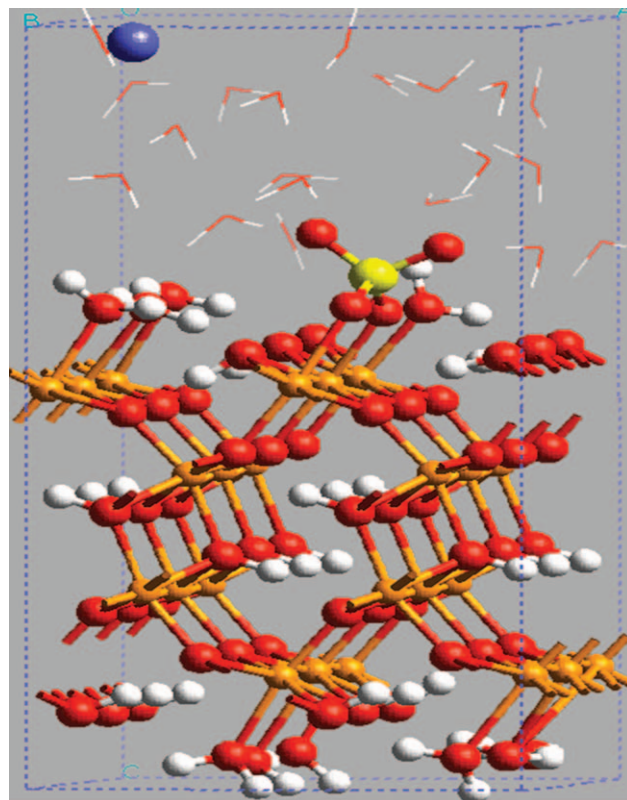


Figure 2 Geometry-optimized inner-sphere bidentate bridging sulphate complex on a hydrated (100) α -FeOOH surface slab. Red, oxygen; white, hydrogen; yellow, sulphur; orange, iron; blue, calcium. Explicit H_2O molecules are represented in stick form.

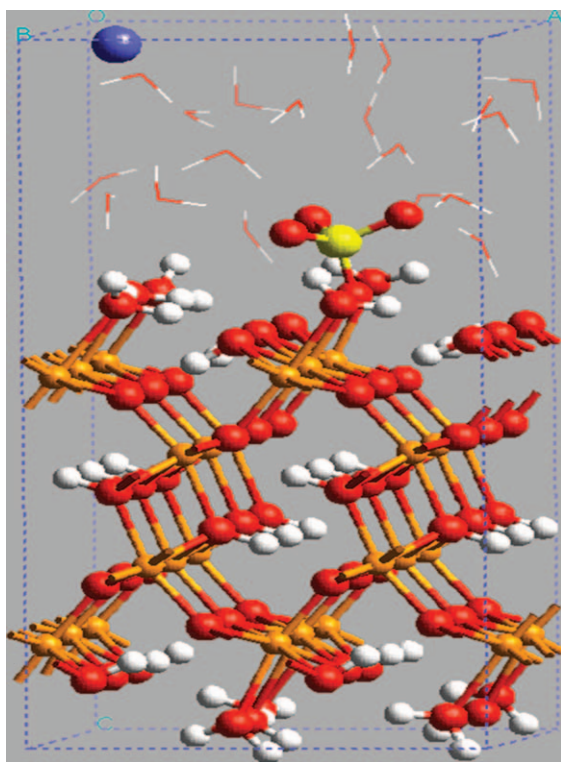


Figure 3 Geometry-optimized inner-sphere monodentate sulphate complex on a hydrated (100) α -FeOOH surface slab. Red, oxygen; white, hydrogen; yellow, sulphur; orange, iron; blue, calcium. Explicit H_2O molecules are represented in stick form.

As previously mentioned, the average Fe–O* bond and Fe–Fe* interatomic distances predicted by the edge-sharing dioctahedral Fe^{3+} cluster models (Table 1) are qualitatively comparable to bulk EXAFS and X-ray diffraction measurements (Waychunas *et al.*, 1996). For example, the predicted average Fe–O* bond distance for the bidentate bridging sulphate complex was 2.01 to 2.03 Å (Table 1), within the experimentally measured range of approximately 1.89–2.12 Å. Likewise, the predicted Fe–Fe* interatomic distance was 3.02–3.08 Å (Table 1), within and slightly outside the upper limit of the experimentally measured range of approximately 2.96–3.07 Å, respectively.

The slightly longer predicted Fe–Fe* interatomic distance of 3.08 Å (Table 1, LanL2DZ/6–311+G(d,p)) was probably related to the coordination of bidentate bridging sulphate and the size of the basis set. To test the effect of basis set size on the predicted Fe–Fe* interatomic distance, the bidentate bridging sulphate cluster model was also geometry-optimized with the LanL2DZ/6–311+G(3df,p) basis set combination (two additional d-polarization functions and one f-polarization function added to the S and O atoms). Geometry optimization of the bidentate bridging sulphate cluster model using the LanL2DZ/6–311+G(3df,p) basis set combination indeed reduced the Fe–Fe* interatomic distance by 0.06 Å (Table 1), within the

experimentally measured range of approximately 2.96–3.07 Å. It is important to note, however, that the LanL2DZ/6–311+G(3df,p) basis set combination did not significantly affect the predicted first shell (S–O and S–O(Fe)), second shell (S–Fe), and (S)O–Fe bond and interatomic distances. Recall that the second shell interatomic distance is an important diagnostic feature of the binding geometry of an oxyanion complex, as determined from an EXAFS measurement.

The average local Fe–O* bond and Fe–Fe* interatomic distances predicted by the (100) α -FeOOH slab model (Table 2) for bidentate bridging sulphate also agreed with experimentally measured values (Waychunas *et al.*, 1996). The predicted average Fe–O* bond and Fe–Fe* interatomic distances were 2.03 and 2.99 Å, within the experimentally measured ranges of approximately 1.89–2.12 Å and 2.96–3.07 Å, respectively (Table 2). Furthermore, the cluster (Table 1, LanL2DZ/6–311+G(3df,p)) and periodic slab (Table 2) DFT predictions of the average Fe–O* bond and Fe–Fe* interatomic distances were also in good agreement (differences < 0.03 Å). The predicted average Fe–O–Fe* and O–Fe–O* bond angles for the cluster and periodic slab DFT calculations agreed to within approximately 2.5–6° (Tables 1 and 2).

Overall, the cluster and periodic slab DFT predictions of the interatomic distances and angles of monodentate sulphate were in good agreement. For example, the predicted second shell S–Fe interatomic distances agreed to within 0.02 Å (Tables 1 and 2). In addition, the predicted first shell S–O and S–O(Fe) bond distances agreed to within 0.02–0.03 Å (Tables 1 and 2). Similar to bidentate bridging sulphate, the (S)O–Fe bond distances predicted by the DFT cluster models were slightly shorter than those predicted by the periodic slab DFT models. It should be noted, however, that the (S)O–Fe bond distance predicted by the LanL2DZ/6–311+G(3df,p) basis set combination (2.14 Å, Table 1) was only 0.02 Å shorter than the (S)O–Fe bond distance predicted by the SP-PBE+U periodic slab DFT calculation (2.16 Å, Table 2).

The average Fe–O* bond and Fe–Fe* interatomic distances predicted by the edge-sharing dioctahedral Fe^{3+} cluster and periodic (100) α -FeOOH slab models for monodentate sulphate were in reasonable agreement and generally within experimentally measured ranges (Tables 1 and 2). The predicted average Fe–O* bond distances agreed to within 0.06–0.08 Å (Tables 1 and 2), and were within the experimentally measured range of approximately 1.89–2.12 Å (Waychunas *et al.*, 1996). The predicted Fe–Fe* interatomic distances agreed to within 0.02–0.07 Å (Tables 1 and 2). Interestingly, the Fe–Fe* interatomic distance predicted by the LanL2DZ/6–311+G(3df,p) DFT cluster model calculation (2.95 Å, Table 1) was 0.01 Å shorter than the lower limit of the experimentally measured range of approximately 2.96–3.07 Å. This may suggest that the slightly longer Fe–Fe* interatomic distance discussed for bidentate bridging sulphate was related to both the coordination of the adsorption complex and the basis set size. The predicted average O–Fe–O* and Fe–O–Fe* bond

angles for the cluster and periodic slab DFT models agreed to within 2.9° and 3.1° , respectively (Tables 1 and 2).

A particularly noteworthy characteristic of the geometry-optimized monodentate sulphate complex was its S–O–Fe bond angle. The S–O–Fe bond angle was predicted to be significantly less than 180° by both the cluster and periodic slab DFT calculations (Tables 1 and 2). A monodentate sulphate complex is generally assumed to adopt C_{3v} point group symmetry. In principle, therefore, a monodentate sulphate complex should exhibit three IR-active vibrational modes: one ν_1 symmetric stretching mode and two ν_3 asymmetric stretching modes (Lefevre, 2004 and references therein). The assumption of a C_{3v} point group restricts the S–O–Fe bond angle to 180° . However, the cluster and periodic slab DFT predictions indicated that monodentate sulphate could form S–O–Fe bond angles significantly less than 180° , thereby adopting lower point group symmetry (within the constraints of a static configuration). P–O–Fe bond angles significantly less than 180° have also been predicted for monodentate phosphate complexes, using DFT cluster model calculations (Kwon & Kubicki, 2004). It is quite possible, however, that a monodentate sulphate complex could freely rotate about its (S)O–Fe bond at room temperature and approximately maintain C_{3v} point group symmetry.

The effect of hydration on the predicted interatomic distances and angles of bidentate bridging and monodentate sulphate was tested by performing DFT cluster model calculations that included 10 explicit H_2O molecules (Table 3, LanL2DZ/6–311+G(d,p)). The corresponding geometry-optimized cluster models are displayed in Figure 4. In addition, the bidentate bridging sulphate cluster model displayed in Figure 1(a) (four explicit H_2O molecules) was geometry-optimized with the IEFPCM method (Table 3). For this particular cluster model, therefore, both explicit and implicit solvation were considered. The predicted average bidentate bridging sulphate (S)O–Fe bond distance increased from 2.03 \AA (four explicit H_2O molecules) to 2.09 \AA when the geometry optimization was performed with 10 explicit H_2O molecules (Tables 1 and 3). The predicted average bidentate bridging sulphate (S)O–Fe bond distance of 2.09 \AA was significantly closer to the values predicted by the periodic slab DFT calculations ($2.15\text{--}2.16 \text{ \AA}$, Table 2). Interestingly, the identical effect was also observed when the geometry optimization included four explicit H_2O molecules and implicit solvation via the IEFPCM method (Table 3). Therefore, the number of explicit H_2O molecules and/or inclusion of implicit solvation significantly influenced the predicted average (S)O–Fe bond distance. It should be noted, however, that the remaining interatomic distances and angles of bidentate bridging sulphate were not significantly affected by an increase in the number of explicit H_2O molecules and/or inclusion of implicit solvation. In a previous investigation, the predicted (Si)O–Fe bond distances of bidentate bridging $\text{H}_2\text{SiO}_4^{2-}$ on an edge-sharing dioctahedral Fe^{3+} cluster model were also shown to be sensitive to the num-

Table 3 Explicit and implicit solvation effects on the interatomic distances and angles of the geometry-optimized bidentate bridging and monodentate sulphate complexes on edge-sharing dioctahedral Fe^{3+} cluster models. Interatomic distances are reported in angstroms (\AA) and bond angles in degrees. *Denotes interatomic distances and angles within the Fe–O–Fe–O ring between the two edge-sharing Fe^{3+} octahedra coordinated to sulphate

	Bidentate SO_4^{2-}		Monodentate SO_4^{2-}
	10 Explicit H_2O molecules	IEFPCM ^c	10 Explicit H_2O molecules
Distance/ \AA			
S–Fe	3.30	3.32	3.40
S–O	1.50	1.49	1.50 (± 0.005)
S–O(Fe)	1.50	1.51	1.50
(S)O–Fe	2.09	2.09	2.11
Fe–Fe* ^a	3.08	3.08	2.96
Fe–O* ^b	2.03 (± 0.04)	2.02 (± 0.04)	1.99 (± 0.03)
Angle/degrees			
S–O–Fe	133.2	133.6	140.3
O–Fe–O*	80.0	79.0	82.0
Fe–O–Fe*	98.8	99.7	96.2

^aExperimental bulk Fe–Fe interatomic distances in Fe (hydr)oxides along single, edge-sharing dioctahedral chains range from approximately 2.96 to 3.07 \AA .

^bExperimental bulk Fe–O and Fe–O(H) bonds bridging two Fe^{3+} octahedra range from approximately 1.89 to 2.12 \AA (Waychunas *et al.*, 1996).

^cCluster model from Figure 1(a) geometry-optimized with the IEFPCM method.

ber of explicit H_2O molecules (Hiemstra & Van Riemsdijk, 2006).

A few differences were noted when the monodentate sulphate complex was geometry-optimized with six versus 10 explicit H_2O molecules (Tables 1 and 3). The predicted monodentate sulphate (S)O–Fe bond distance was actually unaffected by an increase in the number of explicit H_2O molecules, in contrast

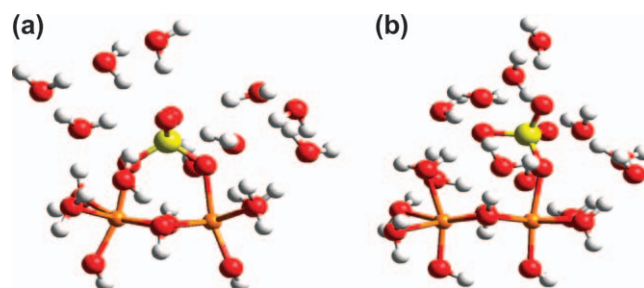


Figure 4 Geometry-optimized inner-sphere sulphate complexes on edge-sharing dioctahedral Fe^{3+} cluster models: (a) bidentate bridging sulphate ($\text{Fe}_2(\text{OH})_4(\text{OH}_2)_4\text{SO}_4(\text{H}_2\text{O})_{10}$) and (b) monodentate sulphate ($\text{Fe}_2(\text{OH})_4(\text{OH}_2)_5\text{SO}_4(\text{H}_2\text{O})_{10}$). Explicit H_2O molecules are H-bonded to the sulphate complexes. Red, oxygen; white, hydrogen; yellow, sulfur; orange, iron.

to the bidentate bridging complex (Tables 1 and 3). Including six explicit H₂O molecules in the DFT geometry optimization may have been sufficient to describe the (S)O–Fe bond distance of monodentate sulphate. On the other hand, the predicted monodentate sulphate S–Fe interatomic distance and S–O–Fe bond angle were affected by an increase in the number of explicit H₂O molecules. The S–Fe interatomic distance and S–O–Fe bond angle decreased from 3.46 to 3.40 Å and 144.7 to 140.3°, respectively, when increasing the number of explicit H₂O molecules by four (Tables 1 and 3). It is reasonable to assume that the monodentate sulphate S–Fe interatomic distance and S–O–Fe bond angle exhibit significant variability due to the rotational flexibility of monodentate complexes.

Conclusions

DFT calculations were performed with edge-sharing dioctahedral Fe³⁺ cluster models and a periodic slab model of the (100) α -FeOOH surface to predict the binding geometries of monodentate and bidentate bridging sulphate complexes. The edge-sharing dioctahedral Fe³⁺ cluster models closely resembled the local structure and composition of the (100) α -FeOOH surface. Interatomic distances and angles predicted by the cluster and periodic slab DFT calculations exhibited good agreement, despite the lack of long-range order in the cluster models. Furthermore, the second shell S–Fe interatomic distances predicted for the bidentate bridging and monodentate sulphate complexes were significantly different (approximately 0.1–0.2 Å). Therefore, EXAFS measurements should be able to distinguish between bidentate bridging and monodentate sulphate complexes, at least on the (100) α -FeOOH surface.

Previous studies have shown that DFT cluster model calculations of As(V) (Ladeira *et al.*, 2001; Sherman & Randall, 2003) and As(III) (Zhang *et al.*, 2005) complexes predicted accurately the first and second shell interatomic distances, as measured by EXAFS. There are probably two principal explanations as to why the DFT cluster model calculations predicted accurately the first and second shell interatomic distances of As(V) and As(III) complexes. First, EXAFS spectroscopy probes the local structure of an adsorption complex and the cluster models are intrinsically local (i.e. lack long-range order). Secondly, as shown by this investigation, the interatomic distances and angles predicted by DFT cluster models agree well with similar (i.e. structure and composition) periodic slab DFT models. In other words, including long-range order may not be a prerequisite to successfully modelling the binding geometries of oxyanion complexes at the mineral–H₂O interface.

An investigation is currently underway to analyse the cluster and periodic slab DFT predictions presented in this investigation, with respect to calculating theoretical photoelectron scattering phase shifts and amplitudes necessary for EXAFS fitting.

It is important to restate that the predicted interatomic distances and angles were derived from geometry optimizations performed on static configurations. At room temperature, the predicted interatomic distances and angles will exhibit variability. This variability, however, can be estimated with *ab initio* molecular dynamics (AIMD) simulations. Constant temperature AIMD simulations of inner- and outer-sphere sulphate complexes are currently in progress.

Acknowledgements

K. W. Paul appreciates financial support from a University of Delaware fellowship. The VASP calculations were performed at the Center for Environmental Kinetics Analysis, a National Science Foundation and Department of Energy Environmental Molecular Sciences Institute at The Pennsylvania State University (NSF Grant No CHE-0431328). The Gaussian 03 calculations were performed at the Delaware Biotechnology Institute, Bioinformatics Center (NSF Grant No EPS-0447610). We appreciate helpful advice from Andrei Bandura and Jorge Sofo regarding the utilization of VASP. We are grateful to Ryan Tappero for a critical review of the manuscript prior to submission. We also appreciate helpful contributions and advice from Daniel Tunega, Glenn Waychunas, Keith Smith, and two anonymous reviewers.

References

- Baltrusaitis, J., Jensen, J.H. & Grassian, V.H. 2006. FTIR spectroscopy combined with isotope labeling and quantum chemical calculations to investigate adsorbed bicarbonate formation following reaction of carbon dioxide with surface hydroxyl groups on Fe₂O₃ and Al₂O₃. *Journal of Physical Chemistry B*, **110**, 12005–12016.
- Bargar, J.R., Kubicki, J.D., Reitmeyer, R. & Davis, J.A. 2005. ATR-FTIR spectroscopic characterization of coexisting carbonate surface complexes on hematite. *Geochimica et Cosmochimica Acta*, **69**, 1527–1542.
- Bargar, J.R., Trainor, T.P., Fitts, J.P., Chambers, S.A. & Brown, G.E. 2004. In situ grazing-incidence extended X-ray absorption fine structure study of Pb (II) chemisorption on hematite (0001) and (1–102) surfaces. *Langmuir*, **20**, 1667–1673.
- Blöchl, P.E. 1994. Projector augmented-wave method. *Physical Review B*, **50**, 17953–17979.
- Brown, G.E. & Sturchio, N.C. 2002. An overview of synchrotron radiation applications to low temperature geochemistry and environmental science. In: *Applications of Synchrotron Radiation in Low-Temperature Geochemistry and Environmental Sciences* (eds P.A. Fenter, M.L. Rivers, N.C. Sturchio & S.R. Sutton), pp. 1–115. Reviews in Mineralogy and Geochemistry, Volume 49. Mineralogical Society of America, Washington, DC.
- Cances, E., Mennucci, B. & Tomasi, J. 1997. A new integral equation formalism for the polarizable continuum model: theoretical background and applications to isotropic and anisotropic dielectrics. *Journal of Chemical Physics*, **107**, 3032–3041.

- Catalano, J.G., Trainor, T.P., Eng, P.J., Waychunas, G.A. & Brown, J.G.E. 2005. CTR diffraction and grazing-incidence EXAFS study of U (VI) adsorption onto $\alpha\text{-Al}_2\text{O}_3$ and $\alpha\text{-Fe}_2\text{O}_3$ (1–102) surfaces. *Geochimica et Cosmochimica Acta*, **69**, 3555–3572.
- Cornell, R.M., Posner, A.M. & Quirk, J.P. 1974. Crystal morphology and the dissolution of goethite. *Journal of Inorganic and Nuclear Chemistry*, **36**, 1937–1946.
- Dudarev, S.L., Botton, G.A., Savrasov, S.Y., Humphreys, C.J. & Sutton, A.P. 1998. Electron-energy-loss spectra and the structural stability of nickel oxide: an LSDA+U study. *Physical Review B*, **57**, 1505–1509.
- Eggleston, C.M., Hug, S., Stumm, W., Sulzberger, B. & Afonso, M.D. 1998. Surface complexation of sulfate by hematite surfaces: FTIR and STM observations. *Geochimica et Cosmochimica Acta*, **62**, 585–593.
- Fendorf, S., Eick, M.J., Grossl, P. & Sparks, D.L. 1997. Arsenate and chromate retention mechanisms on goethite. 1. surface structure. *Environmental Science and Technology*, **31**, 315–320.
- Frisch, M.J., Trucks, G.W., Schlegel, H.B., Scuseria, G.E., Robb, M.A., Cheeseman, J.R. et al. 2003. *Gaussian 03 (Revisions B.05 and D.01)*. Gaussian, Inc, Pittsburgh, PA.
- Gaboriaud, F. & Ehrhardt, J.J. 2003. Effects of different crystal faces on the surface charge of colloidal goethite ($\alpha\text{-FeOOH}$) particles: an experimental and modeling study. *Geochimica et Cosmochimica Acta*, **67**, 967–983.
- Hahn, T. (ed.) 1996. *International Tables of Crystallography*. Kluwer Academic Publishers, Norwell, MA.
- Harrison, J.B. & Berkheiser, V.E. 1982. Anion interactions with freshly prepared hydrous iron-oxides. *Clays and Clay Minerals*, **30**, 97–102.
- Hay, P.J. & Wadt, W.R. 1985. Ab initio effective core potentials for molecular calculations – potentials for the transition-metal atoms Sc to Hg. *Journal of Chemical Physics*, **82**, 270–283.
- Hiemstra, T. & Van Riemsdijk, W.H. 2006. On the relationship between charge distribution, surface hydration, and the structure of the interface of metal hydroxides. *Journal of Colloid and Interface Science*, **301**, 1–18.
- Hug, S.J. 1997. In situ Fourier transform infrared measurements of sulfate adsorption on hematite in aqueous solutions. *Journal of Colloid and Interface Science*, **188**, 415–422.
- Kohn, W. & Sham, L.J. 1965. Self-consistent equations including exchange and correlation effects. *Physical Review*, **140**, A1133–A1138.
- Kresse, G. & Furthmuller, J. 1996a. Efficiency of ab-initio total energy calculations for metals and semiconductors using a plane-wave basis set. *Computational Materials Science*, **6**, 15–50.
- Kresse, G. & Furthmuller, J. 1996b. Efficient iterative schemes for ab initio total-energy calculations using a plane-wave basis set. *Physical Review B*, **54**, 11169–11186.
- Kresse, G. & Joubert, D. 1999. From ultrasoft pseudopotentials to the projector augmented-wave method. *Physical Review B*, **59**, 1758–1775.
- Kwon, K.D. & Kubicki, J.D. 2004. Molecular orbital theory study on surface complex structures of phosphates to iron hydroxides: calculation of vibrational frequencies and adsorption energies. *Langmuir*, **20**, 9249–9254.
- Ladeira, A.C.Q., Ciminelli, V.S.T., Duarte, H.A., Alves, M.C.M. & Ramos, A.Y. 2001. Mechanism of anion retention from EXAFS and density functional calculations: arsenic (V) adsorbed on gibbsite. *Geochimica et Cosmochimica Acta*, **65**, 1211–1217.
- Lefevre, G. 2004. In situ Fourier-transform infrared spectroscopy studies of inorganic ions adsorption on metal oxides and hydroxides. *Advances in Colloid and Interface Science*, **107**, 109–123.
- Manning, B.A., Fendorf, S.E. & Goldberg, S. 1998. Surface structures and stability of arsenic (III) on goethite: spectroscopic evidence for inner-sphere complexes. *Environmental Science and Technology*, **32**, 2383–2388.
- Methfessel, M. & Paxton, A.T. 1989. High-precision sampling for Brillouin-zone integration in metals. *Physical Review B*, **40**, 3616–3621.
- Monkhorst, H.J. & Pack, J.D. 1976. Special points for Brillouin-zone integrations. *Physical Review B*, **13**, 5188–5192.
- Myneni, S.C.B., Traina, S.J., Waychunas, G.A. & Logan, T.J. 1998. Experimental and theoretical vibrational spectroscopic evaluation of arsenate coordination in aqueous solutions, solids, and at mineral–water interfaces. *Geochimica et Cosmochimica Acta*, **62**, 3285–3300.
- Omoike, A., Chorover, J., Kwon, K.D. & Kubicki, J.D. 2004. Adsorption of bacterial exopolymers to $\alpha\text{-FeOOH}$: inner-sphere complexation of phosphodiester groups. *Langmuir*, **20**, 11108–11114.
- Parfitt, R.L. & Smart, R.S.C. 1977. IR-spectra from binuclear bridging complexes of sulfate adsorbed on goethite ($\alpha\text{-FeOOH}$). *Journal of the Chemical Society–Faraday Transactions I*, **73**, 796–802.
- Parfitt, R.L. & Smart, R.S.C. 1978. Mechanism of sulfate adsorption on iron-oxides. *Soil Science Society of America Journal*, **42**, 48–50.
- Paul, K.W., Borda, M.J., Kubicki, J.D. & Sparks, D.L. 2005. Effect of dehydration on sulfate coordination and speciation at the Fe-(hydr) oxide–water interface: a molecular orbital/density functional theory and Fourier transform infrared spectroscopic investigation. *Langmuir*, **21**, 11071–11078.
- Paul, K.W., Kubicki, J.D. & Sparks, D.L. 2006. Quantum chemical calculations of sulfate adsorption at the Al- and Fe-(hydr) oxide– H_2O interface-estimation of Gibbs free energies. *Environmental Science and Technology*, **40**, 7717–7724.
- Peak, D., Ford, R.G. & Sparks, D.L. 1999. An in situ ATR-FTIR investigation of sulfate bonding mechanisms on goethite. *Journal of Colloid and Interface Science*, **218**, 289–299.
- Perdew, J.P., Burke, K. & Ernzerhof, M. 1996. Generalized gradient approximation made simple. *Physical Review Letters*, **77**, 3865–3868.
- Persson, P. & Axe, K. 2005. Adsorption of oxalate and malonate at the water–goethite interface: molecular surface speciation from IR spectroscopy. *Geochimica et Cosmochimica Acta*, **69**, 541–552.
- Pulay, P. 1980. Convergence acceleration of iterative sequences. The case of SCF iteration. *Chemical Physics Letters*, **73**, 393–398.
- Rollmann, G., Rohrbach, A., Entel, P. & Hafner, J. 2004. First-principles calculation of the structure and magnetic phases of hematite. *Physical Review B*, **69**, 165107–165119.
- Sainz-Diaz, C.I., Timon, V., Botella, V. & Hernandez-Laguna, A. 2000. Isomorphous substitution effect on the vibration frequencies of hydroxyl groups in molecular cluster models of the clay octahedral sheet. *American Mineralogist*, **85**, 1038–1045.
- Sherman, D.M. & Randall, S.R. 2003. Surface complexation of arsenic (V) to iron (III) (hydr) oxides: structural mechanism from ab initio molecular geometries and EXAFS spectroscopy. *Geochimica et Cosmochimica Acta*, **67**, 4223–4230.

- Sparks, D.L. 2003. *Environmental Soil Chemistry*, 2nd edn. Academic Press, San Diego, CA.
- Sposito, G. 1998. On points of zero charge. *Environmental Science and Technology*, **32**, 2815–2819.
- Szytula, A., Burewicz, A., Dimitrij, Z., Krasnick, S., Rzany, H., Todorovi, J. *et al.* 1968. Neutron diffraction studies of alpha-FeOOH. *Physica Status Solidi*, **26**, 429–434.
- Tribe, L., Kwon, K.D., Trout, C.C. & Kubicki, J.D. 2006. Molecular orbital theory study on surface complex structures of glyphosate on goethite: calculation of vibrational frequencies. *Environmental Science and Technology*, **40**, 3836–3841.
- Turner, L.J. & Kramer, J.R. 1991. Sulfate ion binding on goethite and hematite. *Soil Science*, **152**, 226–230.
- Watanabe, H., Gutleben, C.D. & Seto, J. 1994. Sulfate-ions on the surface of maghemite and hematite. *Solid State Ionics*, **69**, 29–35.
- Waychunas, G.A., Fuller, C.C., Rea, B.A. & Davis, J.A. 1996. Wide angle X-ray scattering (WAXS) study of ‘two-line’ ferrihydrite structure: effect of arsenate sorption and counterion variation and comparison with EXAFS results. *Geochimica et Cosmochimica Acta*, **60**, 1765–1781.
- Waychunas, G., Trainor, T., Eng, P., Catalano, J., Brown, G., Davis, J. *et al.* 2005. Surface complexation studied via combined grazing-incidence EXAFS and surface diffraction: arsenate on hematite (0001) and (10–12). *Analytical and Bioanalytical Chemistry*, **383**, 12–27.
- Wijnja, H. & Schulthess, C.P. 2000. Vibrational spectroscopy study of selenate and sulfate adsorption mechanisms on Fe and Al (hydr) oxide surfaces. *Journal of Colloid and Interface Science*, **229**, 286–297.
- Wood, D.M. & Zunger, A. 1985. A new method for diagonalising large matrices. *Journal of Physics A: Mathematical and General*, **18**, 1343–1359.
- Yoon, T.H., Johnson, S.B., Musgrave, C.B. & Brown, G.E. 2004. Adsorption of organic matter at mineral/water interfaces. I. ATR-FTIR spectroscopic and quantum chemical study of oxalate adsorbed at boehmite/water and corundum/water interfaces. *Geochimica et Cosmochimica Acta*, **68**, 4505–4518.
- Zhang, N.L., Blowers, P. & Farrell, J. 2005. Evaluation of density functional theory methods for studying chemisorption of arsenite on ferric hydroxides. *Environmental Science and Technology*, **39**, 4816–4822.